Journal of Sound and Vibration 608 (2025) 119082

Contents lists available at ScienceDirect

Journal of Sound and Vibration

journal homepage: www.elsevier.com/locate/jsvi

Wave parameters of an acoustic black hole beam from exact wave-like solutions

Le Chang, Li Cheng *

Department of Mechanical Engineering, The Hong Kong Polytechnic University, Hong Kong, PR China

ARTICLE INFO

Keywords:
Acoustic black hole
wave propagation
wave parameters
exact solution
geometrical acoustics

ABSTRACT

Acoustic black hole (ABH) structures have garnered significant interest due to their unique wave characteristics, encompassing wave velocity reduction, wavelength compression, amplitude augmentation, and energy concentration. Existing wave parameters characterizing ABH features are derived from the geometrical acoustics theory based on local uniformity assumption. Despite their widespread use, they are not rigorously exact and their applicable range remains unknown. Leveraging a tactic variable substitution technique, this paper derives the exact solutions of Bernoulli-Euler ABH beams, cast in a wave-like form. Different from the existing exact solutions, the wave-like form of the solutions allows clear separation of different wave components, thus leading to a full set of explicit analytical expressions of ABH-specific wave parameters including phase velocity, group velocity, wavelength, energy distribution, and energy transport velocity. Valid for the entire frequency range, this new set of exact wave-like solutions allows for the re-assessment of the existing wave parameters based on uniformity assumption to determine their validation range. Meanwhile, the exact wave parameters given by this paper allow for accurate quantification of the ABH effects and inherent physical interpretation of wave motion within an ABH beam, which provides the benchmark and reference solutions for ABH-related research and applications.

1. Introduction

Acoustic black hole (ABH) structures, exemplified by beams or plates with a decreasing thickness profile according to a power-law function$h(x) = \varepsilon x^m (m \geq 2)$, have aroused intensive research interest. When flexural waves travel towards the thin region of an ABH, the wavelength and wave speed of the incident wave gradually decrease as a result of the structural nonuniformity in thickness. In the ideal case where the thickness approaches zero, the phase velocity of the waves becomes zero, thereby annulling wave reflection. Concurrently, wave compression occurs due to the continuous aggregation of wavenumber and the modulation and amplification of wave amplitude, leading to an accumulation and concentration of vibrational energy. These salient features can be made use of in many applications such as wave focusing [1], wave attenuation [2,3], bandgap design [4], acoustic emission detection [5], and the design of medical device/equipment [6], etc.

The unique spatially varying wave properties of the ABH structures pose a significant challenge in accurately determining various wave parameters which are essential for characterizing wave propagation. To tackle this problem, the geometrical acoustics (GA) approximation [7–10] has been widely applied. The pioneering work of Mironov [7] on an ABH beam provided wave parameters based

* Corresponding author.
E-mail addresses: lechang977@gmail.com (L. Chang), li.cheng@polyu.edu.hk (L. Cheng).

https://doi.org/10.1016/j.jsv.2025.119082
Received 6 December 2024; Received in revised form 21 February 2025; Accepted 24 March 2025
Available online 25 March 2025

on the GA, subject to the so-called 'smoothness condition', which stipulates that the wavenumber variation within the ABH should be sufficiently small over a distance of wavelength order [7]. This condition allows for approximating the local wave parameters in the ABH by their counterparts in the uniform structure of the same local cross section. The GA-based wave parameters, abbreviated as GAWPs hereinafter, qualitatively pinpoint the salient features of the ABH. In practical situations where a truncation makes zero thickness unattainable, Krylov and Tilman also used the GA approximation to demonstrate that the wave reflection coefficient can be significantly impaired by applying suitable damping material [11].

Despite its approximative nature, the GA-based theory has been serving as the cornerstone for ABH research, which has been widely applied in the open literature. The acquired understanding based on GAWPs also enabled a significant amount of research on ABH in terms of theoretical and numerical modelling as well as practical applications. Modelling effort includes the wavelet-decomposed method [12,13], the impedance matrix method [14–16], the transfer matrix method [17–20], and the finite element method [4, 21–23], etc. In the long pursuit for exact solutions of the wave equation of ABH structures, the one in the form of power functions to the Bernoulli-Euler equation for an ABH beam with power index m=2 was obtained and applied to calculate the reflection coefficient of bending waves and to perform dynamic analyses [10,24]. For m>2, the exact solution was also represented as hypergeometric series [24]. By deriving the exact solutions of parabolically tapered ABH plate, flexural vibrations [25] in finite circular plates with ABH pit and the scattering of flexural waves [26] within ABH inserted in an infinite thin plate were also studied. These works were also commented on in a comprehensive review on ABH [27]. Note the aforementioned exact solutions take different forms, e.g. power function or hypergeometric series, etc., rather than wave-like ones. Drawing on Euler's experience [28] in studying the exact solutions of uniform beams, it is believed that exact solutions, especially if they can be cast into wave-like form, not only facilitate the resolution of specific dynamic problems but, more crucially, offer an intuitive and generalized depiction of wave propagation patterns before the introduction of specific numerical values. Among other conclusions, the inaccuracy of the GA in predicting the vibrational properties, especially in the low-frequency range was noted [29]. This inaccuracy is understandable, since the GA is established on the assumption of local uniformity, which can only be satisfied in the high frequency range [30]. These observations surmise that the exact solution should be rearticulated to better reflect the underlying wave properties and the wave parameters based on GA approximation, i.e. the GAWPs, should be re-examined and assessed.

The above analysis motivated this study, which offers a twofold contribution. Firstly, we present an exact explicit wave-like solution to the flexural wave equation for ABH beams featuring quadratically varying thickness profiles. Specifically, the solution is expressed in an exponential form rather than the conventional power function representation. This reformulation intrinsically maintains the wave-like physical interpretation while enabling explicit characterization of the wave dynamics, thereby facilitating subsequent quantitative analysis of key wave parameters. Secondly, the full set of wave parameters, including wave amplitude, wavenumber, phase velocity, group velocity, wavelength, energy density, energy flux, and energy transport velocity, is analytically derived from the propagating wave components contained in the wave-like solution. Notably, the entire derivation does not rely on the local uniformity approximation, marking a significant difference from the GA approximation. As the derived new set of wave parameters are the exact product of the exact solutions to the wave equation based on Bernoulli-Euler theory, the parameter group is referred to as the Bernoulli-Euler wave parameters (BEWPs) hereafter. The BEWPs enable accurate quantification of ABH effects and offer a fundamental physical understanding of wave dynamics within an ABH beam, thereby establishing benchmark and reference solutions for future ABH-relevant research and applications.

The paper is organized as follows. The main concepts of the GA and formulations of GAWPs are briefly restated in Section 2. Exact solutions are derived with unidirectional propagating wave components extracted for the derivation of the BEWPs in Section 3.1. The BEWPs are deduced or defined in the remainder of Section 3, thereby quantifying the ABH effects. Numerical examples in Section 4.1 demonstrate the accuracy of the present solution. In Section 4.2, variations of the GAWPs and the BEWPs, including wavelength and wave velocities, are numerically compared across a wide frequency range, to establish the validation limit of the former. Finally, Section 5 concludes the paper.

2. ABH wave parameters approximated by geometrical acoustics

Consider flexural waves in an ABH beam whose thickness varies proportionally to the square of the spatial coordinate x, i.e.$h(x) = \varepsilon x^2$(where$\varepsilon$is a constant) as shown in Fig. 1. The beam has a constant width b. As an approximate theory, the GA theory assumes sufficiently smooth variation of the ABH thickness and equates the local wave properties of the ABH to those of a locally uniform beam of the same cross-section. Consequently, the local wavenumber$k_G(x)$can be represented according to the wavenumber of the uniform beam based on Bernoulli-Euler theory as

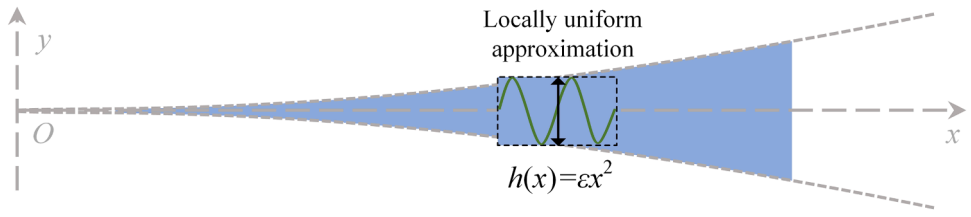

Fig. 1. An ABH beam in *Oxy* coordinate system and the local uniformity assumption of geometrical acoustics.

$$k_G(x) \sim \left(\frac{\rho A(x)\omega^2}{EI(x)}\right)^{\frac{1}{4}} = \left(\frac{12\rho\omega^2}{E\varepsilon^2}\right)^{\frac{1}{4}}\frac{1}{x}, \tag{1}$$

where$\rho$is the mass density;$E$the modulus of elasticity;$A(x) = bh(x)$the cross section area;$I(x) = bh^3(x)/12$the moment of inertia;$\omega$the angular frequency. The subscript 'G' denotes parameters approximated by the GA and the '$\sim$' implies that the wavenumber is approximated.

The criterion for the applicability of this approach generally requires that the spatial variation of local wavenumber should remain minimal across a distance comparable to the wavelength, which can be expressed as the following inequality:

$$\left|\frac{\mathbf{d}k_G(x)}{\mathbf{d}x}\frac{1}{k_G^2(x)}\right| \ll 1. \tag{2}$$

Substitution of$k_G - \omega$relation from Eq. (1) into the smoothness condition, which is expressed in terms of the local wavenumber in Eq. (2), yields the smoothness condition, expressed in terms of frequency as:

$$\omega \gg \varepsilon\sqrt{E/12\rho}. \tag{3}$$

Assuming the above condition is satisfied, the local phase velocity$c_{pG}(x)$and the local group velocity$c_{gG}(x)$write, respectively

$$c_{pG}(x) = \frac{\omega}{k_G} = \left(\frac{E\varepsilon^2\omega^2}{12\rho}\right)^{\frac{1}{4}} = \omega\xi^{-1/4}x, c_{gG}(x) = \frac{\mathbf{d}\omega}{\mathbf{d}k_G} = \left(\frac{4E\varepsilon^2\omega^2}{3\rho}\right)^{\frac{1}{4}}x = 2\omega\xi^{-1/4}x, \tag{4}$$

where

$$\xi = 12\rho\omega^2 / E\varepsilon^2. \tag{5}$$

The local phase velocity and group velocity tend to zero as$x\to 0$which implies zero reflection [7]. The condition of Eq. (3) indicates that the GAWPs become more accurate at higher frequencies [29]. We reiterate that although the GA can provide an intuitive and qualitative interpretation of wave behavior in ABH, this approach is not rigorously exact due to the imposed smoothness condition [9] and the local uniformity treatment. At low frequencies where the smoothness condition is not satisfied and local uniformity is questionable, wave parameters of the wave behavior in ABH remain theoretically unknown.

3. Exact solution without local uniformity assumption and wave parameters for a quadratic ABH beam

3.1. Exact wave-like solutions for flexural wave motion in ABH beams

To disclose the wave parameters underlying the wave equation for flexural wave motion in the ABH beam, we first derive the exact solution in wave-like form. Considering a quadratic and symmetric ABH profile in a lossless medium, the differential equation for the flexural wave in such structural waveguide based on Bernoulli-Euler theory reads [31]

$$\frac{\partial^2}{\partial x^2}\left[EI(x)\frac{\partial^2 w}{\partial x^2}\right] + \rho A(x)\frac{\partial^2 w}{\partial t^2} = 0, \tag{6}$$

where$w$represents the transverse displacement. Assuming harmonic oscillation

$$w(x,t) = W(x)\exp(\mathbf{i}\omega t), \tag{7}$$

where$W$is the amplitude of$w$and$\mathbf{i}$the imaginary unit, one has

$$\frac{\partial^2}{\partial x^2}\left[EI(x)\frac{\partial^2 W}{\partial x^2}\right] - \omega^2\rho A(x)W = 0. \tag{8}$$

Using the analytical quadratic form of $h(x)$ in $A(x)$ and $I(x)$ gives

$$x^4\frac{\mathbf{d}^4W}{\mathbf{d}x^4} + 12x^3\frac{\mathbf{d}^3W}{\mathbf{d}x^3} + 30x^2\frac{\mathbf{d}^2W}{\mathbf{d}x^2} - \xi W(x) = 0, \tag{9}$$

where$\xi$is defined in Eq. (5). Eq. (9) is a differential equation with variable coefficients. Through a variable substitution [24–26],

$$z = \ln x, \tag{10}$$

Eq. (9) is cast into an equation with constant coefficients as

$$\frac{\mathbf{d}^4W}{\mathbf{d}z^4} + 6\frac{\mathbf{d}^3W}{\mathbf{d}z^3} + 5\frac{\mathbf{d}^2W}{\mathbf{d}z^2} - 12\frac{\mathbf{d}W}{\mathbf{d}z} - \xi W(z) = 0. \tag{11}$$

Then we may assume a trial solution in the form$W = \exp(rz)$to obtain the following characteristic equation as

$$r^4 + 6r^3 + 5r^2 - 12r - \xi = 0, \tag{12}$$

whose roots write

$$r_{1,2} = -\frac{3}{2} \pm \mathbf{i}k_1, r_{3,4} = -\frac{3}{2} \pm k_2, \tag{13}$$

where

$$k_1 = \sqrt{-17/4 + \sqrt{\xi + 4}}, k_2 = \sqrt{17/4 + \sqrt{\xi + 4}}. \tag{14}$$

Obviously,$r_{3,4}$are always real numbers which imply two non-propagating terms of wave solutions$b_{n2}^-$and b_{n2}^+, respectively written as

$$b_{n2}^- = x^{-3/2}\mathbf{exp}(k_2 \ln x), b_{n2}^+ = x^{-3/2}\mathbf{exp}(-k_2 \ln x), \tag{15}$$

in which the superscripts '-' and '+' denote the propagation directions.$r_{1,2}$can be either real or imaginary numbers, depending on the frequency values. If the frequency makes$k_1 \in \mathbb{I}$where$\mathbb{I}$is the set of imaginary numbers, that is,

$$\omega < \omega_0 = \frac{5}{8}\sqrt{\frac{3E\varepsilon^2}{\rho}} \Rightarrow k_1 \in \mathbb{I}, \tag{16}$$

the solutions contain another two non-propagating wavesb_{n1}^- andb_{n1}^+:

$$b_{n1}^- = x^{-3/2}\mathbf{exp}(\overline{k_1} \ln x), b_{n1}^+ = x^{-3/2}\mathbf{exp}(-\overline{k_1} \ln x), \tag{17}$$

where

$$\overline{k_1} = \sqrt{17/4 - \sqrt{\xi + 4}}, \tag{18}$$

and the subscript '$n1$' and '$n2$' denote non-propagating wave related to$\overline{k_1}$andk_2, respectively. The frequency$\omega_0$in Eq. (16) was firstly discovered and discussed by Mironov [10], indicating a threshold frequency value above which waves start to propagate. If the frequency makesk_1a real number, it implies two propagating wavesb^-andb^+given by

$$b^- = x^{-3/2}\mathbf{exp}(k_1 \ln x), b^+ = x^{-3/2}\mathbf{exp}(-k_1 \ln x). \tag{19}$$

In summary, the wave solution containing propagating terms is the linear combination of four waves:

$$W(x) = c_1 b^- + c_2 b^+ + c_3 b_{n2}^- + c_4 b_{n2}^+, \omega > \omega_0, \tag{20}$$

where$c_1 \sim c_4$are undetermined coefficients. Note that the variable substitution is only valid in the case of a quadratic ABH profile in a lossless medium. Clearly, the exact solutions derived above can be cast into the exact solution given by [10,24]. However, the proposed wave-like solutions lead to essential improvements in physical interpretation by separating wave components.

To study the spatially varying properties of waves in the ABH beam, we extractb^-, the left-going propagating term, as the wave function which conforms to the wave-like form [32]:

$$w(x,t) = A_E(x)\mathbf{exp}(\mathbf{i}\varphi_E(x,t)), \tag{21}$$

where$A_E(x)$is the amplitude;$\varphi_E(x,t)$the phase; and the subscript 'E' signifies that the parameters are one of the BEWPs which are disclosed, deduced, and defined from the exact solution of the wave equation based on the Bernoulli-Euler theory. They are expressed by

$$A_E(x) = x^{-3/2}, \varphi_E(x,t) = k_1 \ln x + \omega t. \tag{22}$$

Different from the classical wave solution [33],$\mathbf{exp}(\mathbf{i}(kx + \omega t))$, in which k is the wavenumber, the wave-like interpretation generally allows the wave amplitude and the phase to be spatially related due to the nonuniformity of the structure. More specifically, the first-order derivative of phase with respect to x is no longer a constant, which means the distance between successive maxima (or minima) is not constant. The BEWPs, including wave amplitude, wavenumber, phase velocity, group velocity, wavelength, energy density, energy flux, and energy transport velocity, are to be derived or defined in the following sections, thanks to the wave-like interpretation of the propagating wave in ABH beam.

3.2. Amplitude, dispersion relation, phase velocity, and group velocity

3.2.1. Amplitude

The wave function of Eq. (21) pinpoints the wave amplitude augmentation arising from the ABH effects: the wave amplitude along ABH beam is inversely proportional to$x^{3/2}$.

3.2.2. Wavenumber and dispersion relation (ω-k relation)

According to the kinematic derivation in a nonuniform structure [32], the wavenumber can be defined as the first-order partial derivative of the phase with respect to the space variable. Thus, we define the wavenumber k_E for the flexural waves in the ABH beam as

$$k_E(x) = \frac{\partial \varphi}{\partial x} = \frac{k_1}{x}. \tag{23}$$

Substitution for k_1 in terms of frequency gives the dispersion relation:

$$\omega = \Omega(k_E) = \sqrt{\frac{E\varepsilon^2}{12\rho}\left[\left(k_E^2 x^2 + 17/4\right)^2 - 4\right]}. \tag{24}$$

3.2.3. Phase velocity

The phase velocity can be derived as

$$c_{pE}(x) = \frac{\omega}{k_E} = \frac{\omega}{k_1} x. \tag{25}$$

The phase velocity can also be derived as a product of constant phase. Even though the propagating waves in the ABH beam are dispersive, monochromatic and unidirectional waves still satisfy the constant phase condition during their propagation within the ABH beam. To keep the phase in Eq. (22) constant, the total differential of the phase function must be zero, which is

$$\mathbf{d}\varphi_E = \left(\frac{\partial \varphi_E}{\partial x}\right)\mathbf{d}x + \left(\frac{\partial \varphi_E}{\partial t}\right)\mathbf{d}t = \frac{k_1}{x}\mathbf{d}x - \omega \mathbf{d}t = \mathbf{0}, \tag{26}$$

which yields the phase velocity

$$c_{pE}(x) = \left|\frac{\mathbf{d}x}{\mathbf{d}t}\right| = \frac{\omega}{k_1} x. \tag{27}$$

3.2.4. Group velocity

The group velocity can be derived as

$$c_{gE}(x) = \frac{\mathbf{d}\omega}{\mathbf{d}k_E} = 2\omega k_1 \xi^{-1/2} x, \tag{28}$$

where $\xi = 12\rho\omega^2/E\varepsilon^2$. To derive the group velocity in accordance with constant phase, we consider a wave packet composed of two wave solutions expressed by w_1 and w_2 with the real part taken into consideration:

$$\begin{aligned} w_1 &= x^{-3/2}\cos(k_1 \ln x + \omega t), \\ w_2 &= x^{-3/2}\cos[(k_1 + \Delta k_1)\ln x + (\omega + \Delta\omega)t]. \end{aligned} \tag{29}$$

They share the same amplitude $x^{-3/2}$ but differ slightly in ω and thus k_1, which means

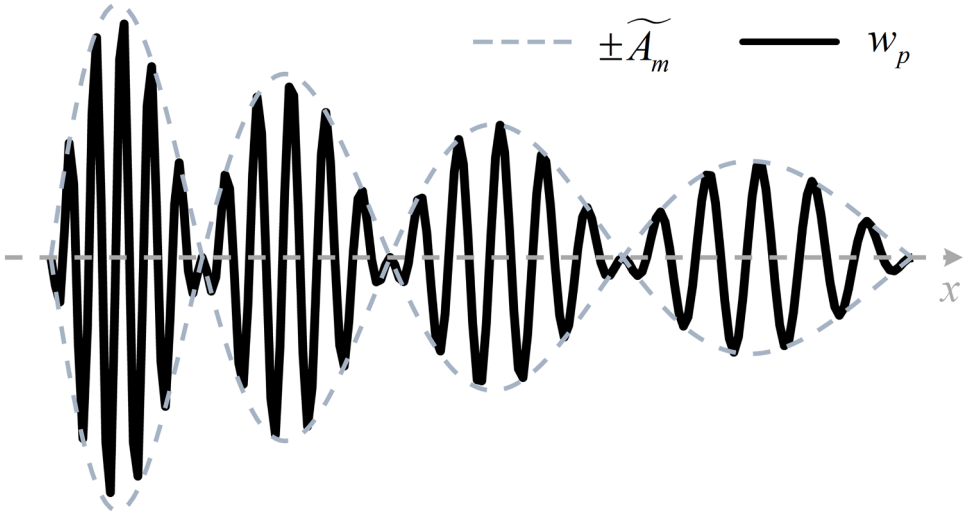

Fig. 2. Diagram of the superposition of two waves in ABH beam. The black solid line represents the superimposed wave. The silver dashed line represents the modulated amplitude. The primary waves move with the phase velocity c_{pE} while the wave packet propagates at group velocity c_{gE}.

$$\Delta k_1 \ll k_1, \Delta\omega \ll \omega. \tag{30}$$

Similar to other linear wave-bearing structures, the superposition principle gives a resultant wave w_p by:

$$\begin{aligned} w_p &= w_1 + w_2 \\ &= 2x^{-3/2}\cos\left(\frac{\Delta k_1 \ln x + \Delta\omega t}{2}\right)\cos\left(k_1 \ln x + \omega t + \frac{\Delta k_1 \ln x + \Delta\omega t}{2}\right) \\ &\sim 2x^{-3/2}\cos\left(\frac{\Delta k_1 \ln x + \Delta\omega t}{2}\right)\cos(k_1 \ln x + \omega t), \end{aligned} \tag{31}$$

which indicates a superimposed wave at frequency$\omega$with a modulated amplitude. In Fig. 2, the superimposed wave is presented in a black solid line and the modulated one by a silver dashed line. Clearly, a large number of primary waves occur within a segment of the wave packet. Each of the primary waves moves with the phase velocity c_{pE}. The propagation of the wave packet$\widetilde{A_m}$follows the modulated amplitude as

$$\widetilde{A_m} = 2x^{-3/2}\cos\left(\frac{\Delta k_1 \ln x + \Delta\omega t}{2}\right). \tag{32}$$

Thus, the constant phase of the modulated amplitude requires

$$\frac{\Delta k_1}{x}\mathbf{d}x + \Delta\omega \mathbf{d}t = 0, \tag{33}$$

which can be applied to the definition of the group velocity of the wave packet as

$$c_{gE}(x) = \left|\frac{\mathbf{d}x}{\mathbf{d}t}\right| = \frac{\Delta\omega}{\Delta k_1}x \to \frac{\mathbf{d}\omega}{\mathbf{d}k_1}x = 2\omega k_1 \xi^{-1/2}x. \tag{34}$$

Note that both the phase velocity and the group velocity derived from the exact solution are proportional to x, in consistent with the GAWPs. Thus, the classical GA descriptions on the ABH effects firstly suggested by Mironov [7], including the reduction of velocity, infinite transit time towards the tip, and zero reflection, are qualitatively correct, and phenomenologically verified by the present exact solutions. However, the constant phase condition examines the phase velocity and group velocity, thereby implying that the phase and group velocities given by the GA do not strictly fulfill the condition.

3.3. Wavelength evolution

The GA utilizes the wave parameters of locally uniform beams to describe waves within the ABH beam. The wavelength thus writes

$$\lambda_G(x) = \frac{2\pi}{k_G(x)} = \frac{2\pi}{\xi^{1/4}}x. \tag{35}$$

Upon closer examination of the distances between local maxima of the wave function, one can observe that for any point x, there

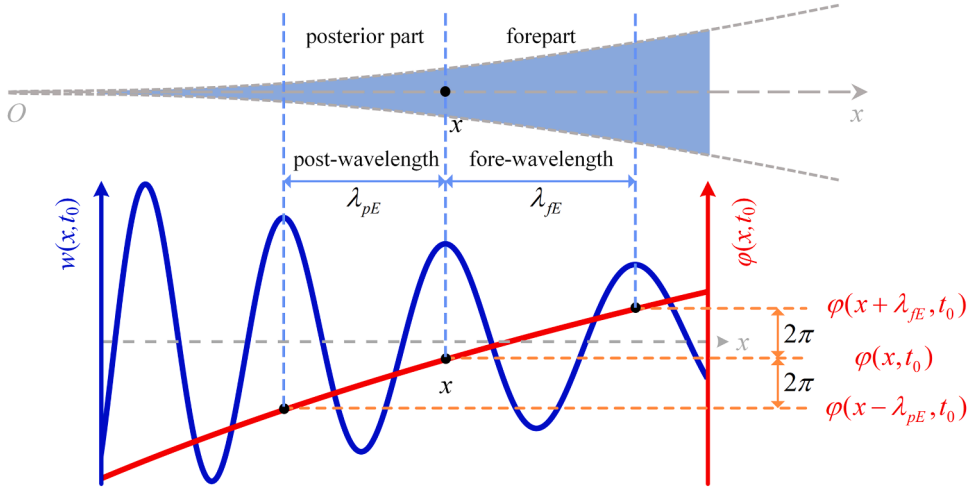

Fig. 3. Diagram of the definition of wavelength in ABH beam. The blue solid line denotes the wave function. The red solid line denotes the phase. Time is frozen at t_0. For any point x, the spatial distances required to achieve a phase shift of 2π towards the forepart and posterior part are referred to as the fore-wavelength$\lambda_{fE}$and the post-wavelengthλ_{pE}, respectively.

are two nearest neighbors with a phase shift of 2π, one towards the forepart and the other towards the posterior part. The distances of these two points from x are evidently different, as shown in Fig. 3. Thus, we define two wavelengths at one point x due to the nonuniformity of the ABH beam. The distance between x and its neighbor with a phase shift of 2π towards the thinner part is expressed by the fore-wavelengthλ_{fE}, and that with its opposite neighbor by the post-wavelengthλ_{pE}. At a given time t_0, the phase shift condition requires that:

$$\varphi_E(x,t_0)-\varphi_E\left(x-\lambda_{fE},t_0\right)=2\pi, \tag{36}$$

$$\varphi_E\left(x+\lambda_{pE},t_0\right)-\varphi_E(x,t_0)=2\pi. \tag{37}$$

3.3.1. Wavelength

By employing the phase expression, Eq. (22), the post-wavelength$\lambda_{pE}$and the fore-wavelengthλ_{fE}can be deduced as

$$\lambda_{pE}(x)=[1-\exp(-2\pi/k_1)]x, \tag{38}$$

$$\lambda_{fE}(x)=[\exp(2\pi/k_1)-1]x. \tag{39}$$

3.3.2. Wavelength compression ratio

The ratio between the post-wavelength$\lambda_{pE}$and the fore-wavelengthλ_{fE}can be used to describe the wave compression, which writes

$$r_0=\frac{\lambda_{pE}}{\lambda_{fE}}=\exp(-2\pi/k_1). \tag{40}$$

Note$r_0$is independent of space and time. Thus, the wavelength of the propagating waves towards the ABH tip decreases geometrically with a constant rate. Also note that the commonly used notion of 'half-wavelength' is not exactly the half of the wavelength due to the nonuniformity of the beam. But the variation of the phase of the half-wavelength is still halved, thus one can just replace 2π with π when studying half-wavelength. Additionally, the formulation of fore-wavelength and post-wavelength defined within traveling waves are also valid for standing waves, as verified in Section 4.1.

3.4. Energy propagation

Consider the left-going propagating waves in the ABH beam whose displacement is expressed by Eq. (21). The kinetic and potential energy densities (energy per unit length) are [34]

$$\boldsymbol{E}_k=\frac{1}{2}\rho A(x)\left[\mathbf{Re}\left(\frac{\partial w}{\partial t}\right)\right]^2=\frac{b\varepsilon\rho\omega^2}{2x}\sin^2(k_1\ln x+\omega t), \tag{41}$$

$$\boldsymbol{E}_p=\frac{1}{2}EI(x)\left[\mathbf{Re}\left(\frac{\partial^2 w}{\partial x^2}\right)\right]^2=\frac{b\varepsilon\rho\omega^2}{2x}\sin^2(k_1\ln x+\omega t+\phi),\phi=\arctan\frac{15-4k_1^2}{16k_1}, \tag{42}$$

where $\mathbf{Re}(z)$denotes the real part of z. For harmonic motion, the time-averaged energy densities write

$$\langle\boldsymbol{E}_k\rangle=\frac{\omega}{2\pi}\int_0^{2\pi/\omega}\boldsymbol{E}_k(x,t)\mathbf{d}t=\frac{b\varepsilon\rho\omega^2}{4x}, \tag{43}$$

$$\langle\boldsymbol{E}_p\rangle=\frac{\omega}{2\pi}\int_0^{2\pi/\omega}\boldsymbol{E}_p\mathbf{d}t=\frac{b\varepsilon\rho\omega^2}{4x}. \tag{44}$$

3.4.1. Time-averaged energy density

The equality of the time-averaged kinetic energy density and time-averaged potential energy density conforms to the principles of energy balance [35] for purely propagating waves. A simple summation yields the total time-averaged energy density as:

$$\langle\boldsymbol{E}\rangle=\frac{b\varepsilon\rho\omega^2}{2x}. \tag{45}$$

Thus, the energy concentration of the ABH effects can be characterized by the total energy density: the total energy per unit length accumulates towards the tip in an inversely proportional manner. The energy flux can be attributed to two primary sources: firstly, the shear force acting through deflection, and secondly, the bending moment acting through section rotation. The shear force V and bending moment M are given by$M=EI(x)\partial^2 w/\partial x^2andV=-\partial M/\partial x$, respectively.

3.4.2. Time-averaged energy flux

Thus, the time-averaged active energy flux for propagating bending waves in an ABH beam is given by [36]

$$\langle \boldsymbol{P} \rangle = \frac{\omega}{2\pi} \int_0^{2\pi/\omega} \mathbf{Re}(V)\mathbf{Re}\left(\frac{\partial w}{\partial t}\right) + \mathbf{Re}(M)\mathbf{Re}\left(\frac{\partial^2 w}{\partial x \partial t}\right) \mathbf{d}t = \frac{Eb\varepsilon^3 \omega}{12} k_1 \sqrt{\xi + 4}. \tag{46}$$

3.4.3. Energy transport velocity

Energy transport velocity [36] is defined by the ratio of time-average energy flux to time-average energy density, which in the ABH beam case becomes

$$c_e(x) = \frac{\langle \boldsymbol{P} \rangle}{\langle \boldsymbol{E} \rangle} = 2\xi^{-1}\sqrt{\xi + 4} k_1 \omega x = c_{gE}(x)\sqrt{1 + 4\xi^{-1}} \sim c_{gE}(x). \tag{47}$$

As can be seen, as$x \to 0$,$c_e(x)$goes to 0 due to the linear dependence. The energy transport velocity is expressed in terms of the group velocity. Contrary to the common understanding applicable to uniform structures, the group velocity in a nonuniform beam like ABH beams here, does not rigorously characterize the energy transport speed; instead, it exhibits a high-frequency asymptotic relation.

Note that the energy transport velocity is not exactly equal to the group velocity in the present case. Similar phenomenon was reported in [37] in which bending waves of a tapered one-dimensional waveguide were investigated. The phenomenon, however, remains unexplained. Based on our analysis, we attempt to propose the following explanation. As seen from the derivation process, the group velocity derivation employs the stationary phase condition of wave packets, inherently defining the group velocity as the propagation velocity of a point (which satisfies the stationary phase condition) on the amplitude envelope (Fig. 2). Energy transport velocity is evaluated based on the point corresponding to the maximum amplitude of the wave. In a medium such as uniform beams, these two points precisely overlap, yielding the same values of the energy transport velocity and the group velocity. In a spatially dispersive media (in which the amplitude of the envelope changes) like ABH beams, these two points are slightly offset, because of the amplitude modulation term ($x^{-3/2}$ in Eq. (22)). As a result, the point estimated over the envelope (used for group velocity estimation), slightly away from the maximum amplitude point of the wave (used for energy transport estimation), has a lower value than the maximum amplitude of the wave. Therefore, the estimated group velocity is lower than the energy transport velocity, and the difference reduces when frequencies get higher, all consistent with the theoretical prediction by the proposed wave parameter formula.

Summarizing the above results, the derived parameter group is tabulated in Table 1, providing readers with a full set of exact analytical expressions informing on how geometric and material parameters affects wave propagation of flexural waves in an ABH beam with m=2, particularly in terms of spatial evolution.

4. Discussions and numerical results

In Section 4.1, the displacement field of an ABH beam is computed by using the exact solution and finite element method, as a way to confirm the accuracy of the present exact wave-like solution. In Section 4.2, the GAWPs and the BEWPs are numerically compared to elucidate the application range of the former in terms of frequency.

4.1. Verification of the exact wave-like solution

A bounded ABH beam shown in Fig. 1 is subjected to a harmonic point force excitation. The geometric, material, and excitation parameters are listed in Table 2. The boundary condition is free at both ends of the beam and the harmonic unity point force is applied at the beam tip. A finite element model (FEM) with 800 cubic Lagrange elements in COMSOL Multiphysics 6.2 is used. For the proposed method, the steady-state displacement field of the ABH beam is already formulated by Eq. (20) where the unknown coefficients are

Table 1
ABH wave parameters derived from the exact solutions of the wave equation based on Bernoulli-Euler theory (BEWPs).

BEWPs	Variation law
AmplitudeA_E	$x^{-3/2}$
Wavenumberk_E	k_1/x
Phase velocityc_{pE}	$\omega k_1^{-1} x$
Group velocityc_{gE}	$2\omega k_1 \xi^{-1/2} x$
Wavelength	Fore-wavelengthλ_{fE}: $[\exp(2\pi/k_1) - 1]x$ Post-wavelengthλ_{pE}: $[1 - \exp(-2\pi/k_1)]x$ Wavelength compression ratio r_0: $\exp(-2\pi/k_1)$
Time-averaged energy density$\langle \boldsymbol{E} \rangle$	$b\varepsilon\rho\omega^2/2x$
Time-averaged energy flux$\langle \boldsymbol{P} \rangle$	$Eb\varepsilon^3\omega k_1\sqrt{\xi+4}/12$
Energy transport velocityc_e	$2\omega k_1 \xi^{-1}\sqrt{\xi+4}x$
Variables	$k_1 = \sqrt{-17/4 + \sqrt{\xi+4}}$ $\xi = 12\rho\omega^2/E\varepsilon^2$

determined by the boundary and load conditions. The numerical calculation is conducted using MATLAB.

In Fig. 4, the displacement field distribution is depicted, by a purple straight line from the present method and solid black circles from FEM. Results coincide with each other, which reveals a good agreement between the two methods. The propagating terms ($b^- + b^+$) and non-propagating terms ($b_{n2}^- + b_{n2}^+$) can be identified from the exact solution and they are delineated in Fig. 4 by the green dashed line marked by deep green hollow circles and the red solid line, respectively. In the far field, the deep green hollow circles overlap solid black circles, whereas disparities are evident in the near field. This indicates that the propagating terms make major contributions to the entire displacement field, while the non-propagating terms only have a notable influence at the boundaries. Thus, the ABH effects can be quantified using the BEWPs derived from the propagating wave of the exact wave-like solution: with their salient features like wavelength compression following a geometrical progression, wave amplitude increasing inversely proportional to $x^{3/2}$, and inverse proportionality of the wave energy density concentration. The light dashed line represents the amplitude envelope for the sharply increasing trend of the wave amplitude, particularly in the far field. The wavelength validation is conducted in the next section and the data of energy density is omitted for brevity.

4.2. Comparison of the wave parameters derived from the exact solution and the geometrical acoustics approximation

The GAWPs and the BEWPs including the wavelength, phase velocity, group velocity, and energy transport velocity are numerically compared. We note that the subscribe 'E' and 'G' denote quantities originating from the exact solution based on Euler theory and approximated by the geometrical acoustics, respectively.

The wavelength comparisons between the exact solution, GA, and FEM are shown in Fig. 5 (a). The wave nodes in the displacement field of Fig. 4 using FEM are extracted for the quantification of post-half-wavelength, which is denoted by red squares. The post-half-wavelengthλ_{pE}(Eq. (38) with 2π replaced by π) is plotted by the black solid line. The half-wavelengthλ_G(Eq. (35) divided by two) is drawn using the light dashed line. A good agreement between$\lambda_{pE}$and the FEM results in the far field is observed. The noticeable inconsistency in the near field is caused by the non-propagating waves, which is already illustrated in Section 4.1 in terms of the displacement field. However, there is an undeniable error in the estimation ofλ_G. A more detailed comparison of the wavelength versus the normalized frequency is shown in Fig. 5 (b). The normalized frequency is a ratio$\omega/\omega_0$where$\omega_0$is from Eq. (16). The frequency ratio greater than one implies the presence of propagating waves in the ABH beam. We have mentioned that the applicability of the GA relies on the smoothness condition which requires higher frequencies. The frequency condition can be written in terms of$\omega_0$as

$$\omega / \omega_0 \gg 8 / 15, \tag{48}$$

which is represented by the green line in Fig. 5 (b). The relative error between the post-half-wavelength$\lambda_{pE}$and$\lambda_G$is shown in the black solid line and the relative error of the wavelength$\lambda_{pE}$and$\lambda_G$is plotted in the black dashed line. A clear decreasing trend is found with the increase in frequency. It should be noted that the estimation error of the half-wavelength given by the GA is greater than 5% until the frequency ratio reaches 276, which is marked by red point in Fig. 5 (b). The error decreases very slowly and remains at 5% over a broad frequency range. Moreover, the estimation error for the full wavelength is much larger, exceeding 5% within $500\omega/\omega_0$.

The parameters in Table 2 are used to calculate other wave parameters. Fig. 6 (a) shows the variation of the relative error in terms of phase velocities (c_{pE}andc_{pG}) against the frequency ratio. Relative errors in terms of the group velocities (c_{gE}andc_{gG}) and energy transport velocity$c_e$are compared in Fig. 6 (b). Three relative errors are defined, respectively as

$$\mathbf{RE}(c_{pE}, c_{pG}) = \left|\frac{c_{pE} - c_{pG}}{c_{pE}}\right| \times 100\%, \mathbf{RE}(c_e, c_{gG}) = \left|\frac{c_e - c_{gG}}{c_e}\right| \times 100\%, \mathbf{RE}(c_e, c_{gE}) = \left|\frac{c_e - c_{gE}}{c_e}\right| \times 100\%. \tag{49}$$

In Fig. 6 (a), the relative error betweenc_{pE}andc_{pG}ranges from 0 to 20% with the frequency ratio ranging from 0 to 40. The green dashed line indicates the frequency that must be significantly exceeded to satisfy the smoothness condition, i.e.$0.53\omega_0$, as shown in Eq. (48). The red line corresponds to the frequency$\omega_0$above which propagating waves start to exist. Three red points highlight specific values for the relative error and frequency. In the lower frequency range where$\omega < 5.83\omega_0$, the estimation error of the phase velocity from the GA is greater than 10.0%, which drops significantly below 5.0% when the frequency is larger than$11.49\omega_0$.

Given that the concept of the group velocity has always been considered to signify the speed of energy transport, we assess the errors of the group velocities (c_{gE}andc_{gG}) with respect to the energy transport velocityc_e, rather than comparing the group velocities themselves. The solid black line marked with squares in Fig. 6 (b) indicates the error ofc_{gG}relative to c_e. The solid light line marked with triangles depicts the error ofc_{gE}relative toc_e. As the frequency increases,c_{gE}rapidly approachesc_e. However,c_{gG}converges towards$c_e$at a much slower trend. Once the frequency ratio exceeds 1.62 (which is close to the threshold for the appearance of propagating waves),

Table 2
Geometrical, material and excitation parameters of a free-free ABH beam in Fig. 1.

Geometrical parameters		Material parameters		Excitation parameters	
Thickness	$h(x)$=0.024x^2	Elastic modulus	200 Gpa	Load point	$x_f = x_1$
	$x_1 \le x \le x_2$			Load direction	(0,1)
Width	0.02 m	Density	7850 kg/m^3	Frequency	2 kHz
x_1	0.1			Amplitude	1 N
x_2	0.4	Poisson's ratio	0.3	Displacement field	$x_1 \le x \le x_2$

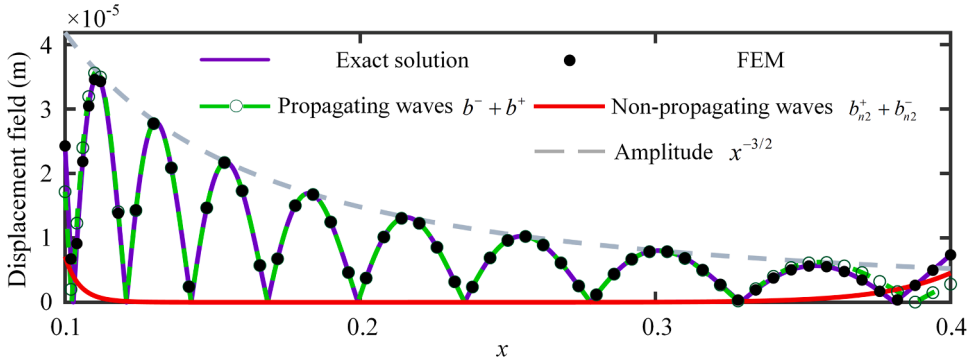

Fig. 4. Displacement field distribution along the ABH beam computed by the present exact solution and FEM. Results reveal a good agreement between FEM and the present method. The propagating terms dominate the entire displacement field.

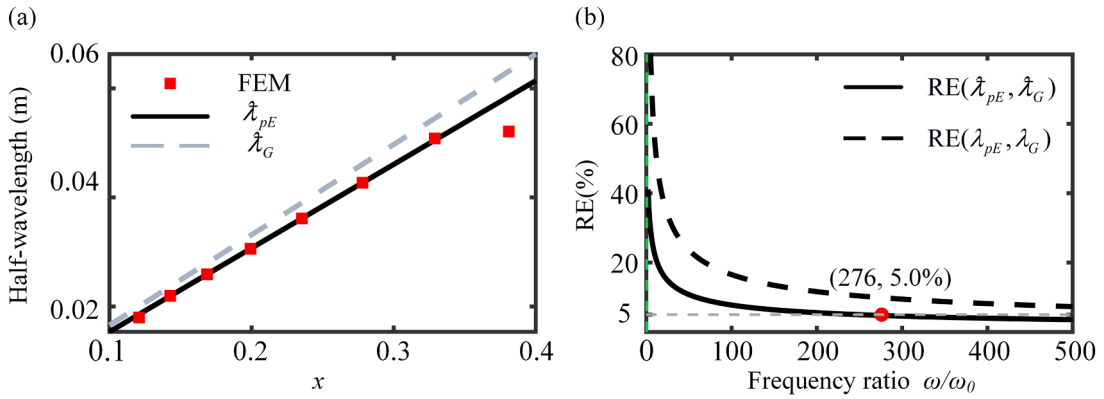

Fig. 5. Comparison of wavelength calculated by the exact solution and the GA. (a) Half-wavelength of the displacement field extracted from Fig. 4. The inconsistency of FEM results and the half-wavelength originating from the exact solution in the near field is caused by the non-propagating waves. (b) A clear disparity of wavelength versus the normalized frequency is observed. The subscribe '*E*' and '*G*' denote quantity originating from the exact solution based on Euler theory and approximated by the geometrical acoustics, respectively.$\hat{\lambda}$andλdenotes the half-wavelength and wavelength, respectively.

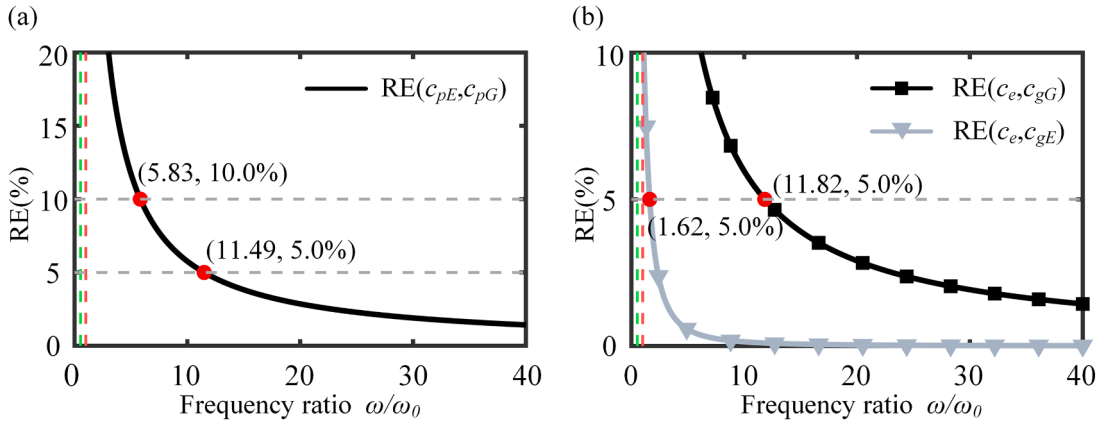

Fig. 6. (a) Relative error of phase velocities: GA result versus exact solution. (b) Relative error of phase velocities originating from the exact solution against the frequency ratio, which is normalized by ω_0 of Eq. (16). The frequency condition derived from the smoothness condition in geometrical acoustics and ω_0 are denoted by green dashed and red dashed lines, respectively. Typical values of the frequency and the relative error are marked by red points.

the error of c_{gE} relative to c_e is less than 5%, whereas it requires the frequency ratio above 11.82 to achieve the same level of accuracy for c_{gG}. With the help of BEWPs, the applicable frequency range of the GA approximation is now accurately quantified from the perspective of wave parameters.

5. Conclusions

The exact wave-like form solution of the wave equation in quadratic ABH beams is derived based on Bernoulli-Euler theory. The obtained wave-like solutions entail better physical interpretability compared with existing power function solutions through clear wave components separation, thereby conducive to disclosing essential wave features. As a result, the full set of wave parameters, describing the salient features of the ABH, are derived from the propagating wave components of the solution without relying on the local uniformity approximation. Main conclusions are summarized as follows:

1). By separating different components in the wave-like solution, wave amplitude function is extracted, which depicts a wave amplitude increase proportional to $x^{-3/2}$.
2). Wavenumber is defined as the first-order partial derivative of the phase with respect to space.
3). The phase velocity and group velocity are deduced. They follow the constant phase condition where the phase of the wave remains unchanged during the propagation.
4). Fore-wavelength and post-wavelength are defined due to the nonuniformity of the ABH beam. Expressions are derived using the phase shift condition. Wavelength evolution is found to follow geometrical progression described by a ratio between the two wavelength components.
5). Energy density intensifies towards the tip of the ABH beam, inversely proportional to the distance from the tip. The energy transport velocity asymptotically equals the group velocity.

The ABH effects can be specified and quantified by the above wave parameters including zero reflection (in ideal zero tip thickness), amplitude increase, wavelength compression, and energy concentration.

The solution is numerically confirmed and the wave parameters derived from the exact solutions and geometrical acoustics approximation are numerically compared. It is shown that the widely used geometrical acoustic solution offers acceptable estimation of wave parameters only at high frequencies, roughly over $12\omega_0$ given by Eq. (16). Therefore, the exact wave parameters given by this paper allow for accurate quantification of the ABH effects and inherent physical interpretation of wave motion within ABH beams, which provides the benchmark and reference solutions for ABH-related research and applications.

Note the current work does not consider structural damping or any added damping treatment, the effects of which have been extensively elaborated in the literature. We believe that, under the lossless assumption, the theoretical work reported in this paper, reveals the most fundamental and salient features pertinent to the ABH-specific wave propagation in an ABH beam. Should damping be considered, we expect that, apart from the wave amplitude, other wave parameters discussed in the paper may not be significantly affected. This, however, warrants more concerted effort as future research.

CRediT authorship contribution statement

Le Chang: Writing – review & editing, Writing – original draft, Validation, Software, Methodology, Investigation, Formal analysis.
Li Cheng: Writing – review & editing, Writing – original draft, Supervision, Resources, Methodology, Conceptualization.

Declaration of competing interest

The authors declare that they have no known competing financial interests or personal relationships that could have appeared to influence the work reported in this paper.

Acknowledgements

We appreciate insightful discussions with Dr. Shuowei An and comments from the reviewers.

Data availability

Data will be made available on request.

Reference

[1] A. Mousavi, M. Berggren, L. Hägg, E. Wadbro, Topology optimization of a waveguide acoustic black hole for enhanced wave focusing, J. Acoust. Soc. Am. 155 (2024) 742–756.
[2] T. He, C. Guo, J. Fu, Y. Bao, X. Liu, Enhancing acoustic emission wave attenuation at structural boundaries: Introducing an additional spiral acoustic black hole and assessing its performance, Ultrasonics 141 (2024) 107353.
[3] L. Ma, L. Cheng, Vibration and sound radiation of an acoustic black hole plate immersed in heavy fluid, J. Acoust. Soc. Am. 154 (2023) 179–190.
[4] F. Gautier, A. Pelat, Broadband vibration mitigation using a two-dimensional acoustic black hole phononic crystal, J. Acoust. Soc. Am. 155 (2024) 3051–3059.

[5] J. Fu, T. He, Z. Liu, Y. Bao, X. Liu, A novel waveguide rod with acoustic black hole for acoustic emission signal enhancement and its performance, Ultrasonics 138 (2024) 107260.
[6] C. Chen, Y. Tang, W. Ren, Y. Wang, J. Guo, S. Lin, Acoustic black hole ultrasonic scalpel, Ultrasonics 143 (2024) 107417.
[7] M. Mironov, Propagation of a flexural wave in a plate whose thickness decreases smoothly to zero in a finite interval, Sov. Phys. Acoust. 34 (1988) 318–319.
[8] V.V. Krylov, Conditions for validity of the geometrical-acoustics approximation in application to waves in an acute-angle solid wedge, Sov. Phys. Acoust. 35 (1989) 176–180.
[9] V.V. Krylov, Geometrical-acoustics approach to the description of localized vibrational modes of an elastic solid wedge, Sov. Phys. Tech. Phys. 35 (1990) 137–140.
[10] M. Mironov, Exact solutions of equation of transverse vibrations for a bar with a specific cross section variation law, Acoust. Phys. 63 (2017) 1–6.
[11] V.V. Krylov, F.J.B.S. Tilman, Acoustic 'black holes' for flexural waves as effective vibration dampers, J. Sound Vib. 274 (2004) 605–619.
[12] L. Tang, L. Cheng, H. Ji, J. Qiu, Characterization of acoustic black hole effect using a one-dimensional fully-coupled and wavelet-decomposed semi-analytical model, J. Sound Vib. 374 (2016) 172–184.
[13] S. Zhang, L. Cheng, On the efficacy of the wavelet decomposition for high frequency vibration analyses, J. Sound Vib. 380 (2016) 213–223.
[14] V.B. Georgiev, J. Cuenca, F. Gautier, L. Simon, V.V. Krylov, Damping of structural vibrations in beams and elliptical plates using the acoustic black hole effect, J. Sound Vib. 330 (2011) 2497–2508.
[15] G. Raybaud, J.Y. Lee, W. Jeon, A. Pelat, F. Gautier, On the control of the absorption of an Acoustic Black Hole by using attached point supports, J. Sound Vib. 548 (2023) 117562.
[16] J.Y. Lee, W. Jeon, Wave-based analysis of the cut-on frequency of curved acoustic black holes, J. Sound Vib. 492 (2021) 115731.
[17] M.X. He, Y. Tang, Q. Ding, Dynamic analysis and optimization of a cantilevered beam with both the acoustic black hole and the nonlinear energy sink, J. Intell. Mater. Syst. Struct. 33 (2022) 70–83.
[18] S. Park, W. Jeon, Ultra-wide low-frequency band gap in a tapered phononic beam, J. Sound Vib. 499 (2021) 115977.
[19] X. Li, Q. Ding, Analysis on vibration energy concentration of the one-dimensional wedge-shaped acoustic black hole structure, J. Intell. Mater. Syst. Struct. 29 (2018) 2137–2148.
[20] Y. Yu, X. Jia, H. Ouyang, Y. Du, Y. Peng, Dynamic properties investigation of an acoustic black hole beam with dynamic vibration absorber based on analytical method, J. Sound Vib. (2023) 118053.
[21] L. Ma, T. Zhou, L. Cheng, Acoustic Black hole effects in Thin-walled structures: Realization and mechanisms, J. Sound Vib. 525 (2022) 116785.
[22] H. Ji, B. Han, L. Cheng, D.J. Inman, J. Qiu, Frequency attenuation band with low vibration transmission in a finite-size plate strip embedded with 2D acoustic black holes, Mech. Syst. Signal Process. 163 (2022) 108149.
[23] T. Zhou, J.-D. Chazot, E. Perrey-Debain, L. Cheng, Performance of the Partition of Unity Finite Element Method for the modeling of Timoshenko beams, Comput. Struct. 222 (2019) 148–154.
[24] J.Y. Lee, W. Jeon, Exact solution of Euler-Bernoulli equation for acoustic black holes via generalized hypergeometric differential equation, J. Sound Vib. 452 (2019) 191–204.
[25] D.J. O'Boy, V.V. Krylov, Damping of flexural vibrations in circular plates with tapered central holes, J. Sound Vib. 330 (2011) 2220–2236.
[26] O. Aklouche, A. Pelat, S. Maugeais, F. Gautier, Scattering of flexural waves by a pit of quadratic profile inserted in an infinite thin plate, J. Sound Vib. 375 (2016) 38–52.
[27] A. Pelat, F. Gautier, S.C. Conlon, F. Semperlotti, The acoustic black hole: A review of theory and applications, J. Sound Vib. 476 (2020) 115316.
[28] L. Euler, De curvis elasticis, Bousquet, Lausanne and Geneva, 1744.
[29] T. Zhou, J.-D. Chazot, E. Perrey-Debain, L. Cheng, Partition of Unity Finite Element Method for the modelling of Acoustic Black Hole wedges, J. Sound Vib. 475 (2020) 115266.
[30] V.V. Krylov, Overview of localised flexural waves in wedges of power-law profile and comments on their relationship with the acoustic black hole effect, J. Sound Vib. 468 (2020) 115100.
[31] U. Lee, Spectral element method in structural dynamics, J. Wiley & Sons Asia, Singapore; Hoboken, NJ, 2009.
[32] G.B. Whitham, Linear and nonlinear waves, Wiley, New York Chichester Weinheim, 1999.
[33] M.J. Benacquista, J.D. Romano, Classical Mechanics, Springer International Publishing, Cham, 2018.
[34] F.J. Fahy, P. Gardonio, Sound and structural vibration: radiation, transmission and response, 2nd ed, Elsevier/Academic, Amsterdam London, 2007.
[35] Y. Lase, M.N. Ichchou, L. Jezequel, ENERGY FLOW ANALYSIS OF BARS AND BEAMS: THEORETICAL FORMULATIONS, J. Sound Vib. 192 (1996) 281–305.
[36] G. Diener, Energy transport in dispersive media and superluminal group velocities, Phys. Lett. A 235 (1997) 118–124.
[37] S.-K. Lee, B.R. Mace, M.J. Brennan, Wave propagation, reflection and transmission in non-uniform one-dimensional waveguides, J. Sound Vib. 304 (2007) 31–49.